Supplementary Figures

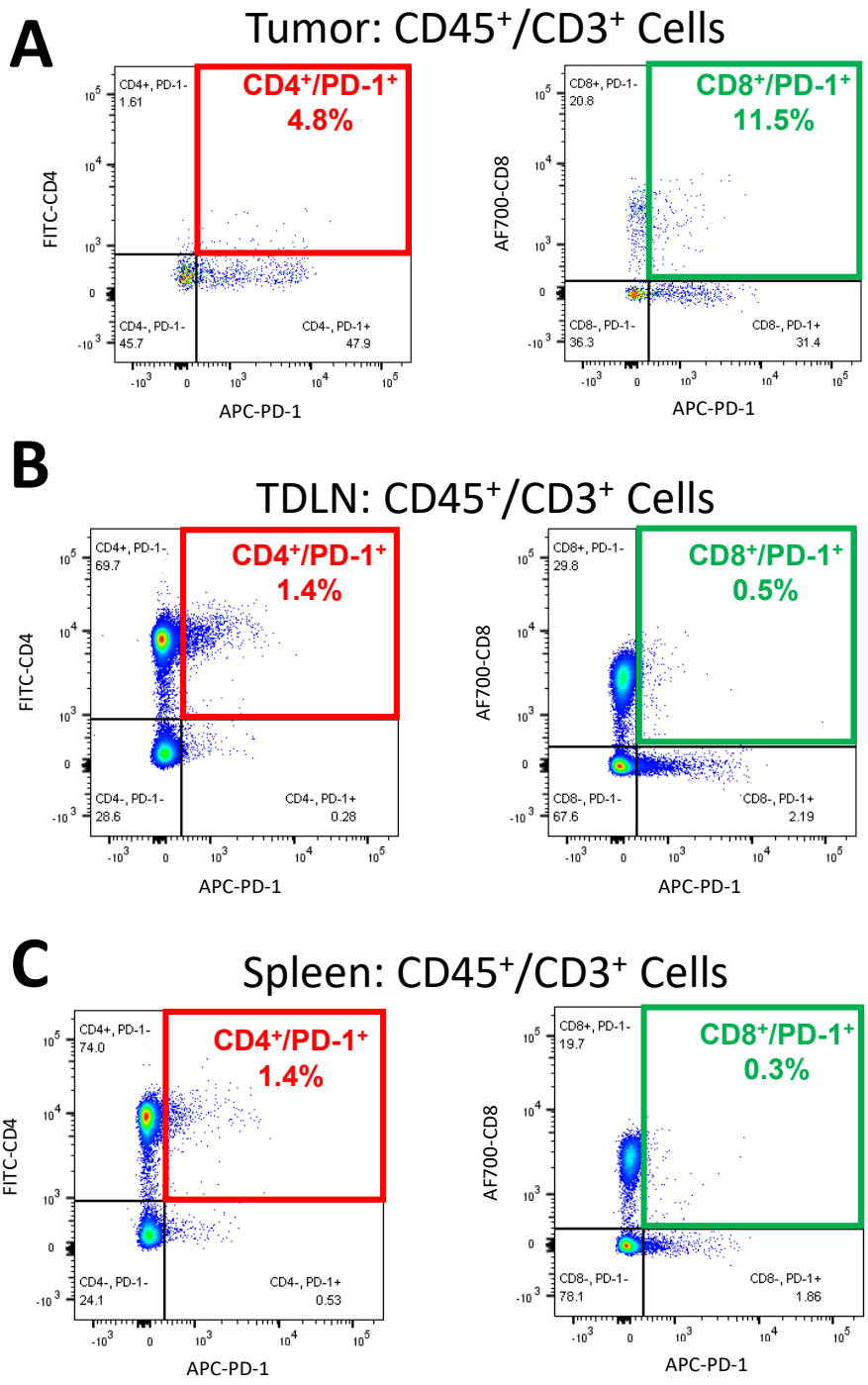

Supplemental Figure 1. Expression of PD-1 on T-cells in the tumor, draining lymph nodes and spleen. Mice were orthotopically transplanted with syngeneic *neu* deletion line (NDL) tumor biopsies in the fourth and ninth mammary fat pads. After tumors reached 5-7 mm (day 21), tumors, draining lymph nodes and spleen were harvested from mice, dissociated, stained for T-cell populations and PD-1 and quantified via flow cytometry (n=3). Levels of T-cells co-expressing CD4 or CD8 and PD-1 in the (**A**) tumor, (**B**) tumor draining lymph node and (**C**) spleen, as a percentage of the pre-gated total T-cell population ($CD45^+$,$CD3^+$ cells).

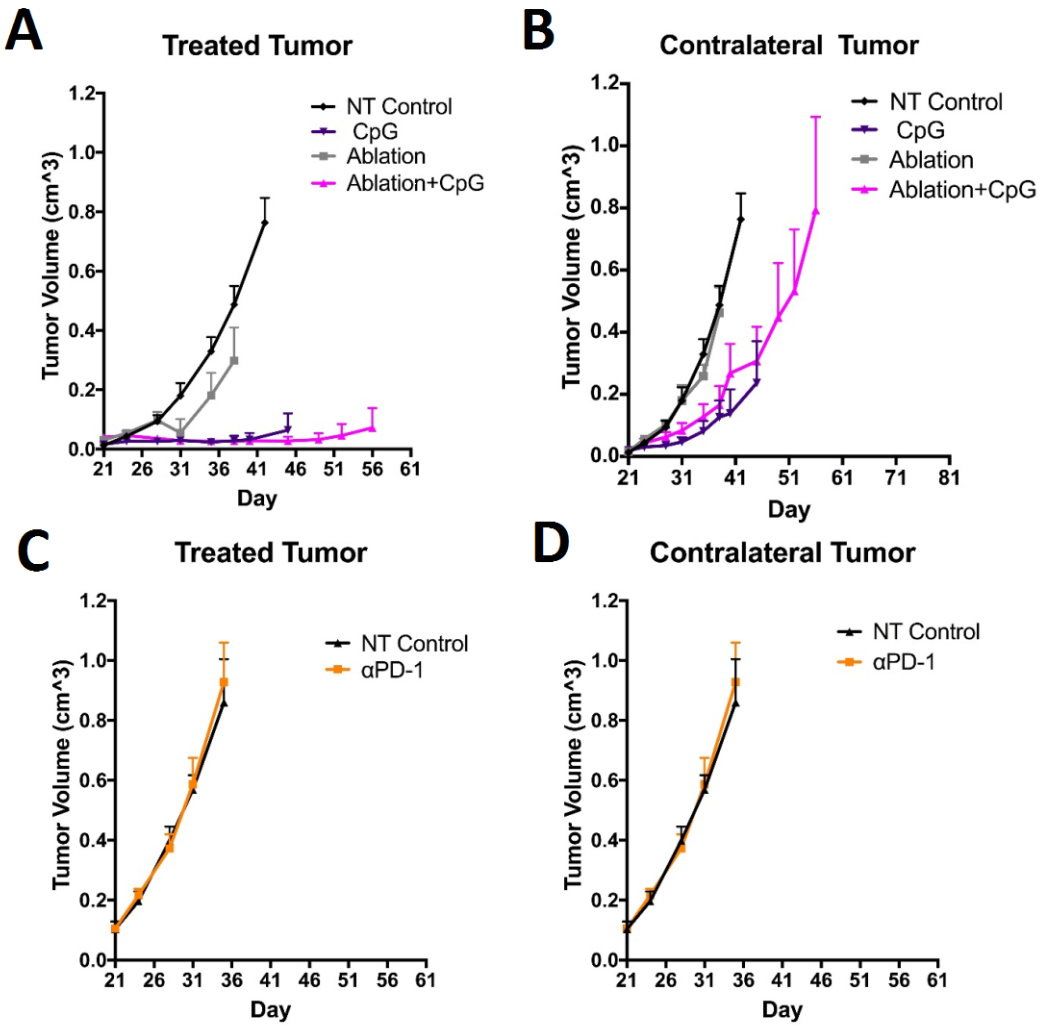

Supplemental Figure 2. Tumor suppression of Ablation+CpG, CpG and αPD-1. (**A-B**) Mice were orthotopically transplanted with syngeneic NDL tumor in the fourth and ninth mammary fat pad and received the therapeutic protocol described in Figure 3A. Treatments included CpG (n=8), αPD-1 (n=3), Ablation (n=7), Ablation+CpG (n=4) and no treatment (NT) control (n=7). (**A**) Ablation+CpG and CpG each suppressed local tumor growth. (**B**) Contralateral tumor growth was slowed by Ablation+CpG and CpG treatments. (**C-D**) αPD-treatment alone did not alter tumor growth. Data plotted as mean ± SEM.

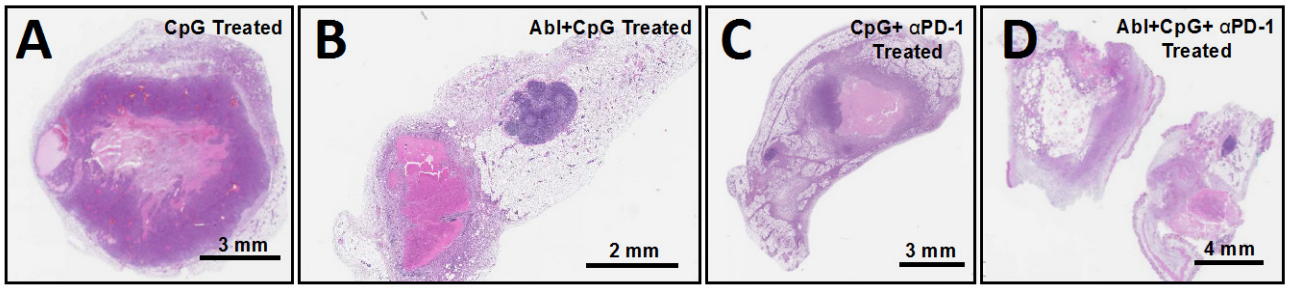

Supplemental Figure 3. Protocols that include thermal ablation induce less-variable local tumor cell death in the treated tumor site. (**A-D**) In mice receiving the therapeutic protocol described in Figure 3A, by day 35, the thermally-ablated treatments (Ablation+CpG and Ablation+CpG+αPD-1) enhanced tumor cell death in the directly-treated tumors as compared to the immunotherapy-alone treatments (CpG and CpG+αPD-1). Representative images of (**A**) CpG-only (n=4), (**B**) Ablation+CpG (n=3), (**C**) CpG+αPD-1 (n=7) and (**D**) Ablation+CpG+αPD-1 (n=3) treated tumors. While thermal ablation reduced the treated tumor growth, the observed effect was transient.

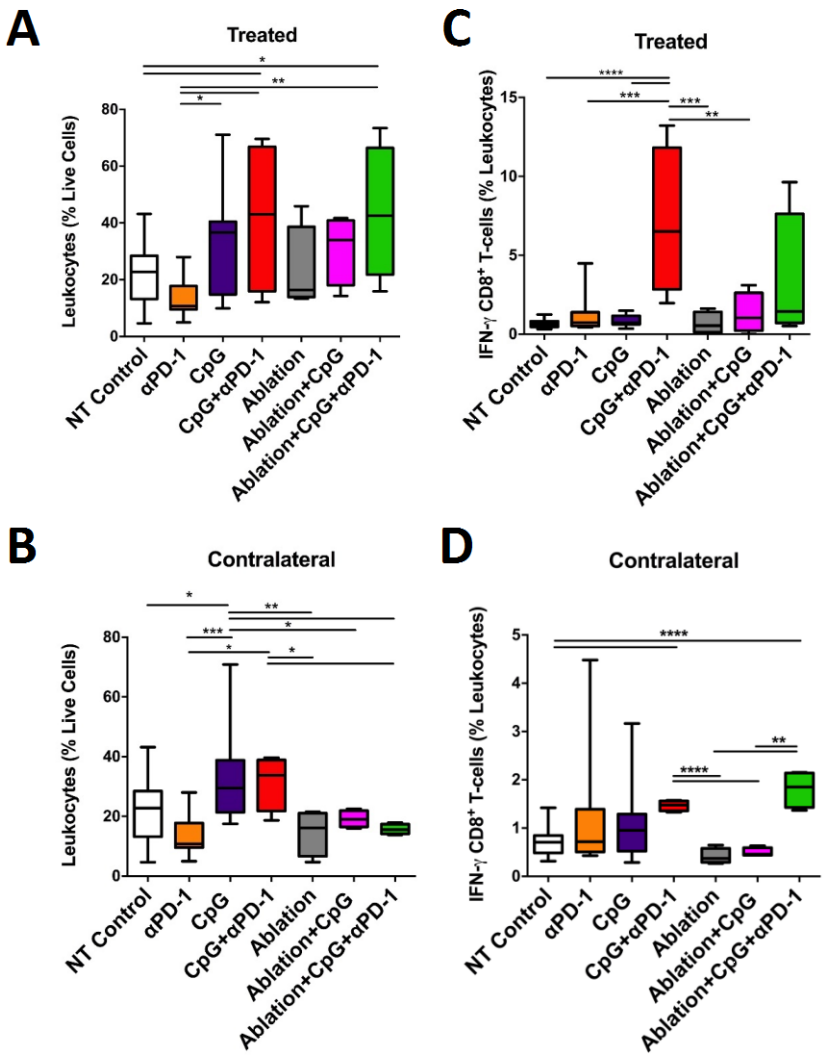

Supplemental Figure 4. Immunocyte fraction in mice treated with thermal ablation coincident with immunotherapy. (**A-D**) Immune cell profiles in the treated and contralateral tumor site following administration of the therapeutic strategy described in Figure 3A. The fourth and ninth mammary fat pads, including the tumor and its embedded lymph node, were harvested at day 28 and compared to all groups via flow cytometry analysis. Data are plotted as mean ± SEM (n=4 per group). (**A**) Elevated leukocytes ($CD45^+$ cells) were observed in the treated tumor for Ablation+CpG+αPD-1 only. (**B**) The addition of thermal ablation lowered the fraction of leukocytes present in the contralateral tumor compared to CpG-immunotherapy protocols without ablation. (**C**) CpG+αPD-1 significantly increased the fraction of interferon gamma (IFN-γ) secreting $CD8^+$ T-cells in the treated tumor. (**D**) Both CpG+αPD-1 and Ablation+CpG+αPD-1 enhanced the fraction of IFN-γ secreting $CD8^+$ T-cells in the contralateral tumor. In these box-and-whiskers plots, the whiskers represent the min and max values, the box boundaries represent the 25^{th} and 75^{th} percentiles, and the middle line is the median value. Significance was determined via one-way ANOVA followed by a Fisher's LSD test without multiple comparisons correction. *$p < 0.05$, **$p < 0.01$, ***$p < 0.001$, ****$p < 0.0001$.

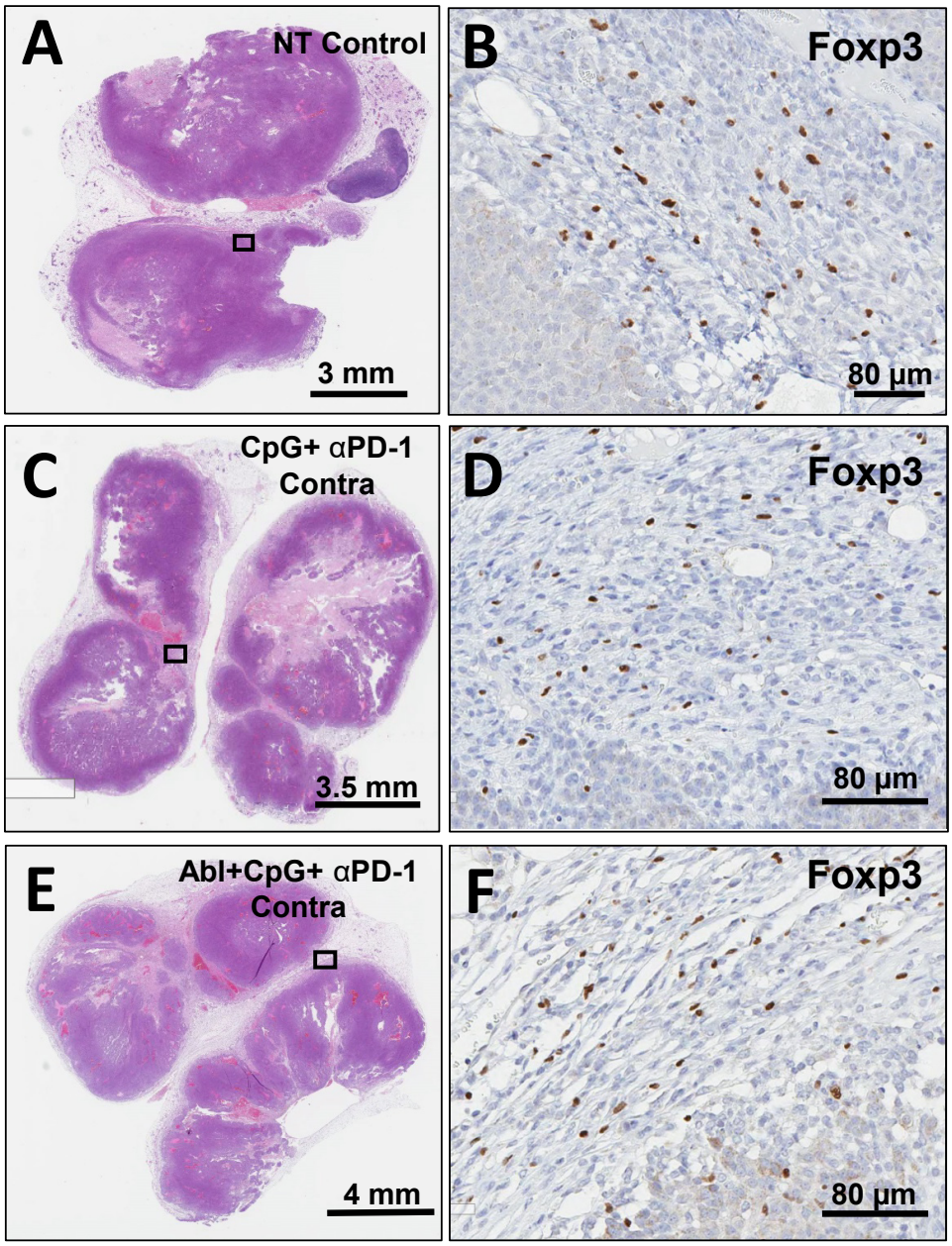

Supplemental Figure 5. Spatial distribution of Regulatory Tcells (Tregs) in the tumor microenvironment. Tregs were visualized by Foxp3 staining at day 50 in NT control tumors, CpG+αPD-1 contralateral tumors and Ablation+CpG+αPD-1 contralateral tumors following the treatment protocol described in Figure 3A. Tregs were distributed evenly throughout the periphery of the tumor among all groups. Representative views of a (**A-B**) NT control tumor, (**C-D**) CpG+αPD-1 contralateral tumor and (**E-F**) Ablation+CpG+αPD-1 contralateral tumor, where black boxes on the hematoxylin and eosin-stained histological tissue sections (**A, C, E**) indicate the respective location of the Foxp3 staining (brown cells) displayed in the corresponding right-column images (n=3 per group).

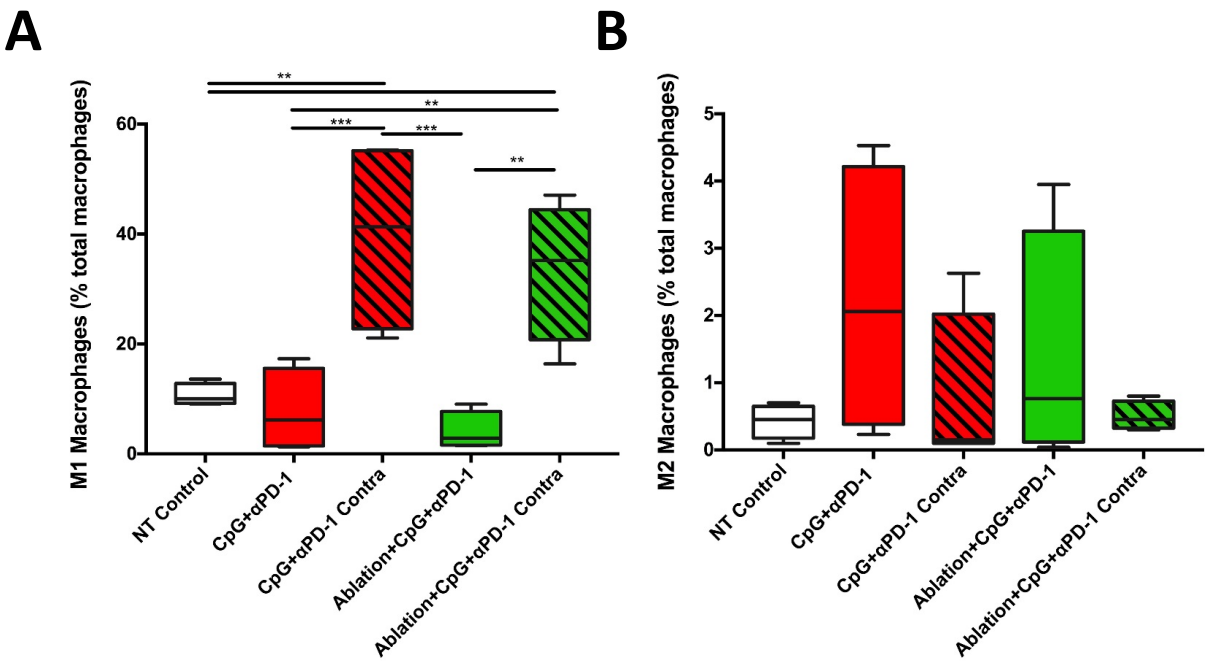

Supplemental Figure 6. Macrophage phenotypes in mice treated with thermal ablation coincident with immunotherapy. (**A-B**) Macrophage phenotypes, as the percent of total macrophages, in the treated and contralateral tumor following administration of the therapeutic strategy described in Figure 3A. The fourth and ninth mammary fat pads, including the tumor and its embedded lymph node, were harvested at day 35 and analyzed via flow cytometry. Data are plotted as mean ± SEM (n=4 per group). (**A**) M1 macrophages were significantly elevated in contralateral tumors for CpG+αPD-1 and Ablation+CpG+αPD-1 treated animals. (**B**) M2 macrophages were elevated in the treated tumor of mice in the CpG+αPD-1 and Ablation+CpG+αPD-1 cohorts. For these box-and-whiskers plots, the whiskers represent the min and max values, the box boundaries represent the 25th and 75th percentiles, and the middle line is the median value. Significance was determined via 1-way ANOVA followed by a Fisher's LSD test without multiple comparisons correction. **p < 0.01, ***p < 0.001.

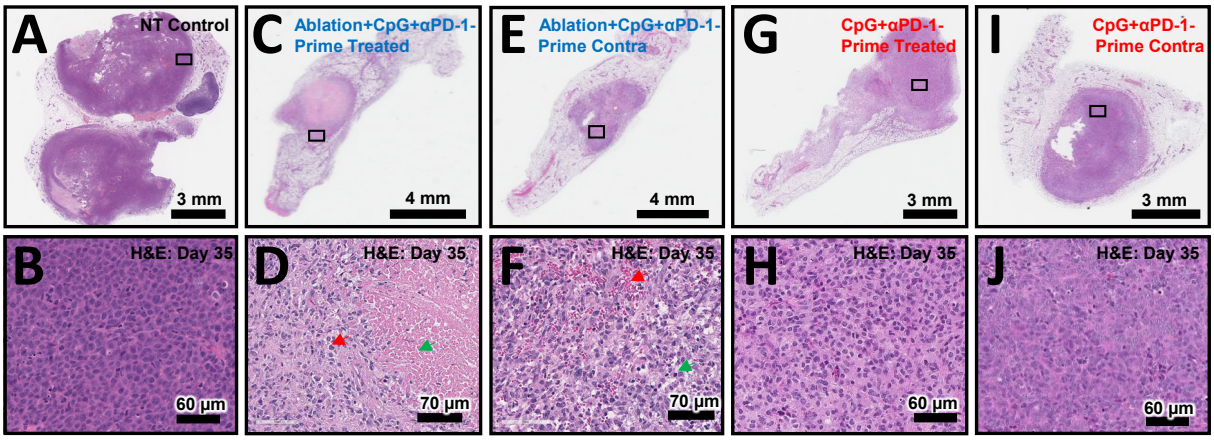

Supplemental Figure 7. Effect of treatment with the priming protocol on the tumor microenvironment. Priming treatment was performed as described in Figure 5A. (**A-J**) By day 35, the thermally-ablated treatment group, Ablation+CpG+αPD-1-Prime, elicited more tumor cell death than the immunotherapy-alone treatment group (n=3 per group). Representative images of (**A**) NT control, (**C**) Ablation+CpG+αPD-1-Prime treated, (**E**) Ablation+CpG+αPD-1-Prime contralateral, (**G**) CpG+αPD-1-Prime treated, and (**I**) CpG+αPD-1-Prime contralateral tumors with black boxes at locations of interest. (**B, D, F, H & J**) Enhanced view of (**B**) NT control, (**D**) Ablation+CpG+αPD-1-Prime treated tumor displaying nonviable tumor tissue with ghosted pyknotic nuclei located in the tumor rim (red arrow), and necrotic tumor cells containing ghosted nuclei located throughout the tumor center (green arrow), (**F**) view of Ablation+CpG+αPD-1-Prime contralateral tumor with evident hemorrhage (red arrow), loss of cell-cell junctions and tumor cell death (green arrow), (**H**) CpG+αPD-1-Prime treated and (**J**) CpG+αPD-1-Prime contralateral tumors showing viable and intact tumor tissue.

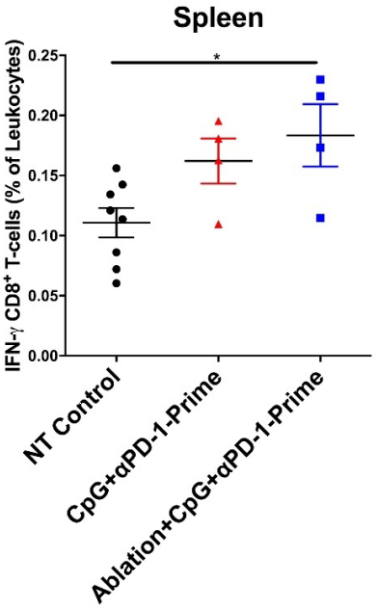

Supplemental Figure 8. IFN-γ CD8⁺ T-cell quantification in the spleen after primed immunotherapy and primed thermo-ablative immunotherapy (TA-immunotherapy). Mice were orthotopically transplanted with syngeneic NDL tumors. Treatments included CpG+αPD-1-Prime, Ablation+CpG+αPD-1-Prime and NT control (n=4 per group). At day 35, spleens were collected for immunocyte quantification via flow cytometry. Only Ablation+CpG+αPD-1-Prime treatment significantly enhanced interferon gamma (IFN-γ) secreting CD8⁺ T-cells in the spleen after treatment compared to NT control. Data plotted as mean ± SEM. Significance was analyzed with 1-way ANOVA followed by a Fisher's LSD test without multiple comparisons correction. *$p < 0.05$.

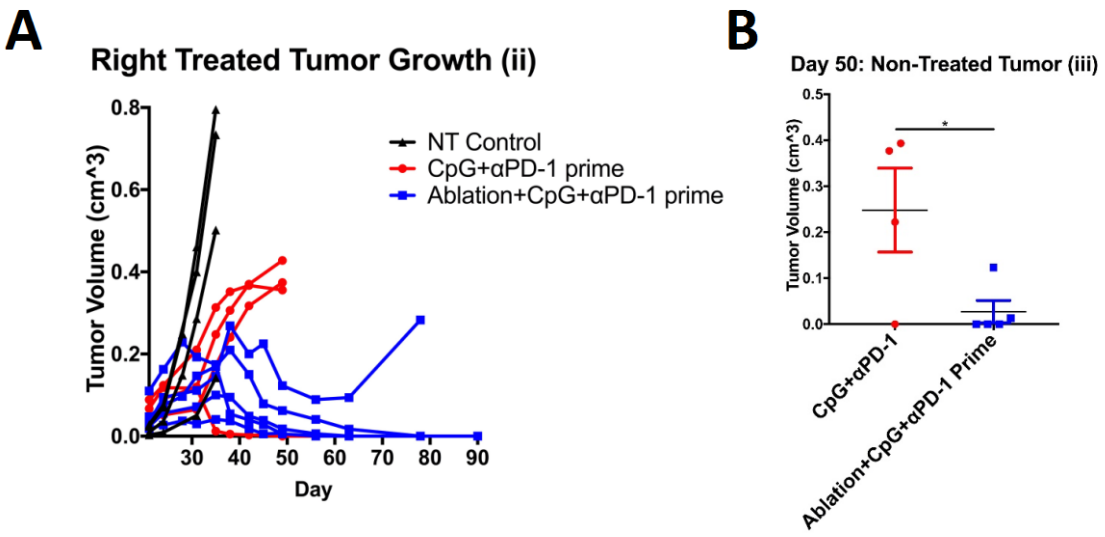

Supplemental Figure 9. Multi-site thermoablative-immunotherapy (TA-immunotherapy). Mice bearing three *neu* deletion line (NDL) tumors were treated with sequential multi-site TA-immunotherapy. Mice were orthotopically transplanted with NDL tumor biopsies in the ninth (i) fourth (ii) and second mammary fat pad (iii), as described previously (see Figure 7. D-E). (**A**) Right-treated tumor growth was followed until an animal from the group was euthanized (tumor diameter >1.5 cm). Treatment cohorts were NT control (n=4), CpG+αPD-1 Prime (n=4) and Ablation+CpG+αPD-1 Prime (n=5). (**B**) Tumor suppression in non-treated tumors was found to be significantly different between CpG+αPD-1 Prime and Abl+CpG+αPD-1 Prime treated animals at day 50. Data plotted as mean ± SEM. Significance was determined via unpaired t-test, *$p < 0.05$.

Supplementary methods

Flow Cytometry

In this syngeneic orthotopic model, a draining lymph node is located within the mammary inguinal fat pad containing the transplanted NDL tumor. Therefore, in studies where the lymph node was not collected and processed separately for analysis, the entire fat pad containing the tumor and inguinal lymph node was processed together. Single-cell suspensions of tumor tissue were obtained by mechanical disruption of the tissue with scissors followed by enzymatic digestion with 1 mg/mL collagenase IV (Sigma Aldrich, St. Louis, MO) for 60 min at 37 ºC and filtration through a 70 µm cell strainer (BD Biosciences, San Jose, CA). Single-cell suspensions of lymphoid organs (spleen and lymph node) were obtained by mechanically grinding the organ through a 70 µm cell strainer in phosphate-buffered saline (PBS), centrifuging and incubating the cells with Ammonium-Chloride-Potassium (ACK) Lysing Buffer (Invitrogen, Carlsbad, CA) for 5 min at room temperature, followed by a final wash with PBS. All cell suspensions were stained using the LIVE/DEAD® Fixable Aqua Dead Cell Stain Kit (Invitrogen, Carlsbad, CA) according to the manufacturer's instructions in order to exclude dead cells from analysis. Cells were then incubated with 2.4G2 mAb for 10 min to block nonspecific antibody binding and finally stained with combinations of the indicated fluorochrome-conjugated anti-mouse antibodies for 25 min at 4 °C. Cells were washed, fixed in 1% PFA Cytofix buffer and run on a LSR II cytometer (BD Bioscience, San Jose CA).

Details on IFN-γ protocol: Briefly, after addition of the IFN-γ catch reagent to cells, followed by incubation in the recommended culture medium for 45 min at 37 °C, cells were washed and incubated with PE-anti-IFN-γ detection antibody in combination with the CD4+/CD8+ T-cell fluorochrome-conjugated antibodies indicated above for 15 min at 4 °C. Finally, cells were washed, fixed in 1% PFA Cytofix buffer and run on a LSR II cytometer.

Histology and Immunohistochemistry

Tissues for microscopic analysis were fixed overnight in 4% buffered formalin and transferred to 70% ethanol the next day. A Tissue-Tek VIP autoprocessor (Sakura, Torrance, CA) was used to process samples for paraffin-embedding. Tissue blocks were then sectioned to 4 µm, sections mounted on glass slides. Hematoxylin and Eosin (H&E) staining was performed at the University of California, Davis, Dept. of Pathology and Laboratory Medicine. For staining of regulatory T cells, the rat-anti-mouse Foxp3 antibody (FJK-16s, eBioscience, San Diego, CA) was used. Cytotoxic T cells were stained with a rat anti-mouse CD8a primary antibody (1:500; 14-0808, eBiosciences). All IHC was performed manually without the use of an automated immunostainer and using the ABC method. Antigen retrieval was performed using a Decloaking Chamber (Biocare Medical, Concord, CA) with citrate buffer at pH 6.0, 125 °C and pressure to 15 psi. The total time slides were in the chamber was 45 min. Incubation with the primary antibody was performed at room temperature overnight in a humidified chamber. Normal goat serum was used for blocking. Biotinylated goat anti-rat (1:500; Vector Labs, Burlingame, CA) was the secondary antibody used with a Vectastain ABC Kit Elite and a Peroxidase Substrate Kit DAB (both from Vector Labs) used for amplification and visualization of signal, respectively. Mouse spleen was used as a positive control. Stained slides were scanned on an AT2 Scanscope (Leica Biosystems) and digital images viewed using the Imagescope program (Leica Biosystems).